Cell

The Neural Circuits and Synaptic Mechanisms Underlying Motor Initiation in *C. elegans*

Beverly J. Piggott,[1,2,4] Jie Liu,[1,4] Zhaoyang Feng,[3,4] Seth A. Wescott,[1] and X.Z. Shawn Xu[1,2,*]
[1]Life Sciences Institute
[2]Department of Molecular and Integrative Physiology
University of Michigan, Ann Arbor, MI 48109, USA
[3]Department of Pharmacology, Case Western Reserve University, Cleveland, OH 44106, USA
[4]These authors contributed equally to this work
*Correspondence: shawnxu@umich.edu
DOI 10.1016/j.cell.2011.08.053

SUMMARY

C. elegans is widely used to dissect how neural circuits and genes generate behavior. During locomotion, worms initiate backward movement to change locomotion direction spontaneously or in response to sensory cues; however, the underlying neural circuits are not well defined. We applied a multidisciplinary approach to map neural circuits in freely behaving worms by integrating functional imaging, optogenetic interrogation, genetic manipulation, laser ablation, and electrophysiology. We found that a disinhibitory circuit and a stimulatory circuit together promote initiation of backward movement and that circuitry dynamics is differentially regulated by sensory cues. Both circuits require glutamatergic transmission but depend on distinct glutamate receptors. This dual mode of motor initiation control is found in mammals, suggesting that distantly related organisms with anatomically distinct nervous systems may adopt similar strategies for motor control. Additionally, our studies illustrate how a multidisciplinary approach facilitates dissection of circuit and synaptic mechanisms underlying behavior in a genetic model organism.

INTRODUCTION

One of the ultimate goals of neuroscience research is to understand how neural circuits and genes generate behavior. Despite the great diversity of their overall anatomy, the basic building blocks of the nervous systems (i.e., structural motifs/modules of neural networks) display similarity across phylogeny (Reigl et al., 2004; Sporns and Kötter, 2004). As such, genetically tractable organisms have emerged as promising models to decode the neural and genetic basis of behavior (de Bono and Maricq, 2005).

The nematode *C. elegans* possesses complex behaviors ranging from motor, sensory, mating, social, sleep, and drug-dependence behaviors to learning and memory (de Bono and Bargmann, 1998; de Bono and Maricq, 2005; Feng et al., 2006; Liu and Sternberg, 1995; Mori and Ohshima, 1995; Raizen et al., 2008). Interestingly, such a complex array of *C. elegans* behaviors, some of which were once thought to be present only in higher organisms, is mediated by a surprisingly small nervous system with merely 302 neurons and ~7,000 synapses (White et al., 1986). *C. elegans* also represents the only organism whose entire nervous system has been completely reconstructed by electron microscopy (EM) (White et al., 1986). These features in conjunction with its amenability to genetic manipulation make *C. elegans* an attractive model for decoding the neural and genetic basis of behavior. However, even for such a simple model organism as *C. elegans*, it remains largely mysterious as to how the nervous system is functionally organized to generate behaviors.

One of the most prominent behaviors in *C. elegans* is its locomotion behavior (de Bono and Maricq, 2005). Locomotion forms the foundation of most, if not all, *C. elegans* behaviors (e.g., sensory, social, mating, sleep, and drug-dependent behaviors, and learning and memory) because these behaviors all involve locomotion and are, to varying degrees, manifested at the locomotion level. During locomotion, worms often initiate backward movement (i.e., reversals) to change the direction of locomotion either spontaneously or in response to sensory cues (de Bono and Maricq, 2005). Previous work from a number of labs has identified several key components in the neural circuitry that controls the initiation of reversals (Alkema et al., 2005; Gray et al., 2005; Hart et al., 1995; Kaplan and Horvitz, 1993; Maricq et al., 1995; Zheng et al., 1999). In particular, a group of command interneurons (AVA, AVD, and AVE) was found to be essential for the initiation of reversals, as laser ablation of the precursors to both AVA and AVD rendered worms incapable of moving backward (Chalfie et al., 1985). Based on the structural map, these command interneurons receive inputs directly from sensory neurons and also from upstream interneurons (first- and second-layer interneurons), and send outputs to ventral cord motor neurons (A/AS type) that drive reversals (Chalfie

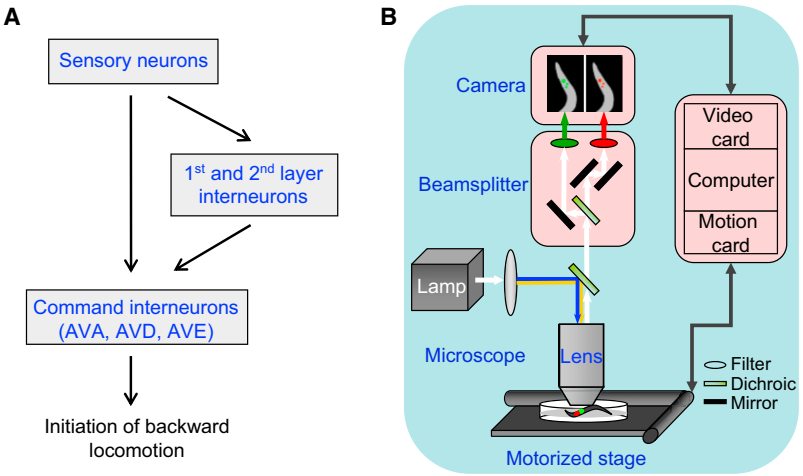

Figure 1. The Current Model of the Locomotion Circuitry that Controls the Initiation of Backward Movement

(A) In this model the command interneurons AVA/AVD/AVE receive input from sensory neurons and interneurons (first layer, AIB/AIA/AIY/AIZ; second layer, RIM/RIA/RIB) and directly synapse onto downstream motor neurons (A/AS, not drawn) to drive backward locomotion.

(B) A schematic drawing of the CARIBN system that enables simultaneous imaging of neuronal activity and behavioral states in freely behaving worms.

See also Figure S1.

et al., 1985; White et al., 1986). Activation of sensory neurons by sensory cues would directly or indirectly excite these command interneurons, leading to the initiation of reversals (de Bono and Maricq, 2005). This constitutes a feed-forward stimulatory circuit (Figure 1A). However, it is not clear whether this circuit, though widely accepted, truly accounts for all of the reversal events seen in this organism.

In this study we applied a multidisciplinary approach to map neural circuits in freely behaving animals. Using this approach, we interrogated the locomotion circuitry and found that our current view of the circuitry needs to be significantly revised. We identified a disinhibitory circuit acting in concert with the command interneuron-dependent stimulatory circuit to control the initiation of reversals. Interestingly, the activity patterns of these two circuits are differentially regulated by sensory cues. Notably, such a dual mode of motor initiation control has also been identified in mammals, suggesting that morphologically distinct nervous systems from distantly related organisms may adopt similar strategies to control motor output. Our study also highlights the value of applying a multidisciplinary approach to dissect the neural and genetic basis of behavior.

RESULTS

Role of Command Interneurons in the Initiation of Reversals during Spontaneous Locomotion

The current model is that the command interneurons AVA, AVD, and AVE, particularly AVA, mediate the initiation of reversals (Figure 1A). As a first step, we imaged the calcium activity of AVA during spontaneous locomotion by expressing in AVA a transgene encoding G-CaMP3.0, a genetically encoded calcium sensor (Tian et al., 2009). DsRed was coexpressed with G-CaMP3.0 to enable ratiometric imaging. To reliably correlate behavior and neuronal activity, we developed an automated calcium imaging system that allows simultaneous imaging of behavior and neuronal calcium transients in freely behaving animals (Figure 1B and Figure S1 available online). We named it the CARIBN (*Ca*lcium *R*atiometric *I*maging of *B*ehaving *N*ematodes) system.

We used the CARIBN system to perform imaging experiments on worms moving on the surface of an NGM (nematode growth media) plate in an open environment without any physical restraint, which is the standard laboratory condition under which nearly all behavioral analyses in *C. elegans* are conducted. Consistent with previous results obtained with a similar system (Ben Arous et al., 2010), we found that AVA exhibited an increase in calcium level during reversals (Figures 2A and 2B), indicating that AVA is involved in controlling backward movement during spontaneous locomotion.

Command Interneurons Are Not Essential for the Initiation of Reversals

To further evaluate the role of the command interneurons AVA/AVD/AVE in reversal initiation, we ablated these neurons individually and in combination. Although worms lacking AVA exhibited a reduced reversal frequency, ablation of AVD or AVE did not result in a notable defect in reversal frequency (Figure 2C), consistent with the view that AVA plays a more important role in triggering reversals than do AVD and AVE (Gray et al., 2005; Zheng et al., 1999). Surprisingly, worms lacking AVA, AVD, and AVE altogether can still efficiently initiate reversals, albeit at a reduced frequency (Figure 2C and Movie S1). These results demonstrate that whereas the command interneurons AVA/AVD/AVE are important for initiating reversals, they are not essential for this motor program. Thus, there must be some unknown circuits that act in parallel to the command interneuron-mediated circuit to regulate the initiation of reversals during locomotion.

RIM Inhibits the Initiation of Reversals, and Its Activity Is Suppressed during Reversals

To identify such circuits, we first examined the wiring pattern of the worm nervous system. RIM, RIA, and RIB are classified as the "second-layer" interneurons that are suggested to act upstream of the command interneurons in the locomotion circuitry (Figure 1A) (Gray et al., 2005). In particular the inter/motor neuron RIM sits at a unique position. It receives input from a number of interneurons and also sends output to downstream head motor neurons and neck muscles (White et al., 1986). Importantly, consistent with previous reports (Alkema et al., 2005; Gray et al., 2005; Zheng et al., 1999), laser ablation of RIM greatly increased reversal frequency (Figure 2C). This

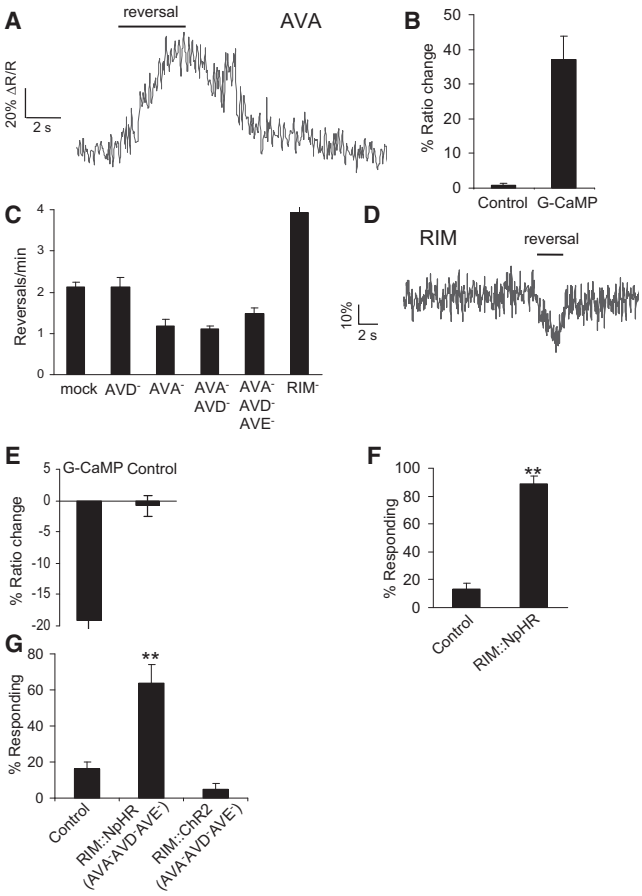

Figure 2. The RIM Neuron Acts to Inhibit the Initiation of Backward Locomotion, and Relieving Such Inhibition Triggers Backward Locomotion

(A) AVA exhibits an increase in calcium level during spontaneous reversals. The bar on top of the trace denotes the time window during which the worm underwent backward movement.

(B) Peak percent change in the ratio of G-CaMP/DsRed fluorescence in AVA during reversals (n = 40). Control, transgenic worms expressing YFP and DsRed under the same promoter.

(C) Laser of ablation of AVA, AVD, AVE, and RIM. AVA/D and AVA/D/E-ablated worms were uncoordinated during reversals (n ≥ 5).

(D) RIM is inhibited during reversals.

(E) Peak percent change in the ratio of G-CaMP/DsRed fluorescence in RIM during reversals (n = 37).

(F) Inhibition of RIM by NpHR triggers reversals. NpHR was expressed as a transgene specifically in RIM. Control worms (transgene-free siblings) showed a basal level of spontaneous reversals. **p < 0.0001 (t test). n = 10.

(G) Inhibition of RIM by NpHR triggers reversals by turning on a parallel pathway. ChR2 was expressed as a transgene specifically in RIM and was turned on with a flash of blue light (2.5–5 mW/mm^2) (n ≥ 5). **p < 0.0001 (ANOVA with the Bonferroni test).

All error bars, SEM.

See also Movie S1.

suggests that RIM inhibits the initiation of reversals during locomotion. By contrast, laser ablation of RIA and RIB does not show a significant effect on reversal frequency during spontaneous locomotion (Gray et al., 2005; data not shown), though these neurons regulate certain sensory behaviors (Mori and Ohshima, 1995).

Therefore, we imaged the activity of RIM during spontaneous locomotion using the CARIBN system. If RIM suppresses the initiation of reversals as suggested above, one would predict that each reversal event should be accompanied by a downregulation of RIM activity. Indeed, RIM activity was downregulated during reversals (Figures 2D and 2E). This result is consistent with the model that RIM inhibits reversal initiation, implying that relieving such inhibition by suppressing RIM activity should trigger reversals.

Suppression of RIM Activity Can Initiate Reversals Independently of AVA/AVD/AVE

To test this, we took an optogenetic approach by expressing halorhodopsin (NpHR) as a transgene specifically in RIM. NpHR is a light-gated chloride pump, and its activation by light suppresses neuronal activity (Zhang et al., 2007). Inhibition of RIM by NpHR effectively triggered reversals in freely moving worms (Figure 2F), suggesting that RIM tonically suppresses reversals during locomotion, and relieving such suppression triggers reversals.

To ascertain whether the role of RIM in reversal initiation depends on the command interneurons AVA/AVD/AVE, we checked worms lacking these neurons. Inhibition of RIM by NpHR can still initiate reversals in AVA/AVD/AVE-ablated worms (Figure 2G). Thus, suppression of RIM activity can trigger reversals independently of the AVA/AVD/AVE-mediated stimulatory circuit. This finding reveals the presence of an RIM-mediated parallel circuit in promoting reversals.

As a control, we performed the converse experiment. If inhibition of RIM can turn on the parallel circuit, stimulation of RIM should not. To test this, we expressed channelrhodopsin-2 (ChR2), a light-gated cation channel (Boyden et al., 2005; Nagel et al., 2005), as a transgene specifically in RIM. To specifically interrogate the role of the parallel circuit, we killed AVA/AVD/AVE to eliminate the stimulatory circuit because it could be artificially turned on by its connections with RIM (Guo et al., 2009). In these worms, stimulation of RIM by ChR2 cannot trigger reversals (Figure 2G). This is in sharp contrast to the observation that inhibition of RIM by NpHR can trigger reversals in the same type of worms (Figure 2G). Thus, RIM inhibition, rather than stimulation, can turn on the parallel circuit to initiate reversals.

Collectively, the aforementioned data suggest that RIM acts in a circuit in parallel to the command interneurons AVA/AVD/AVE to tonically suppress reversals during forward movement, and inhibition of RIM relieves such suppression, leading to reversal initiation.

AIB Acts Upstream of RIM to Trigger Reversals

We next asked which neurons act upstream of RIM to initiate reversals. The wiring map of *C. elegans* nervous system reveals that though over a dozen neurons synapse onto RIM, most of them merely form sparse connections with RIM. Among them, AIB is quite unique in that it is a first-layer interneuron and forms unusually dense synaptic connections with RIM by sending over 30 synapses to RIM (http://www.wormatlas.org) (White et al., 1986). In addition, AIB regulates reversals in olfactory behavior

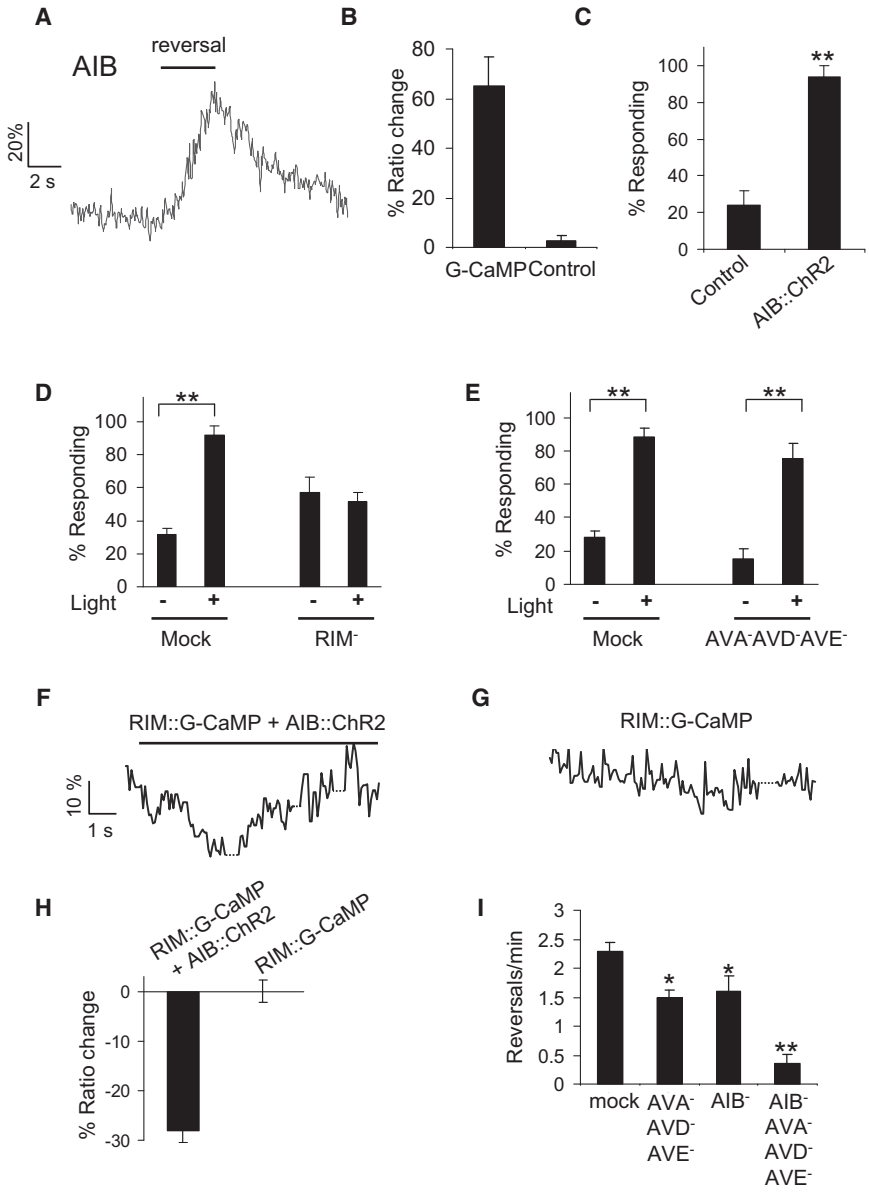

Figure 3. The AIB Neuron Promotes the Initiation of Backward Locomotion by Inhibiting the Activity of RIM

(A) AIB fires during reversals. G-CaMP and DsRed were coexpressed as a transgene specifically in AIB.

(B) Peak percent ratio change in G-CaMP/DsRed fluorescence in AIB during reversals (n = 21). Control worms express YFP and DsRed under the same promoter.

(C) Stimulation of AIB by ChR2 triggers reversals. A flash of blue light was used to trigger reversals in worms expressing ChR2 as a transgene specifically in AIB. Control worms (transgene-free siblings) showed a basal level of spontaneous reversals. **p < 0.0001 (t test). n = 10.

(D) AIB acts upstream of RIM to promote the initiation of reversals. As RIM suppresses reversals, worms lacking RIM showed a higher basal level of spontaneous reversals. **p < 0.0001 (t test). n ≥ 7.

(E) AIB triggers reversals in an AVA/AVD/AVE-independent manner. **p < 0.0001 (t test). n ≥ 9.

(F and G) Calcium imaging of RIM shows that RIM is inhibited by stimulation of AIB. The dotted lines in the traces represent those few missing frames with low image quality, which are refractory to image processing. The bar on top of the trace in (F) denotes the reversal.

(H) Peak percent change in RIM calcium level in response to AIB stimulation by ChR2 (n ≥ 6).

(I) Simultaneous ablation of AVA/AVD/AVE and AIB abolished nearly all reversal events during spontaneous locomotion. AVA/AVD/AVE data are a duplicate from Figure 2C. *p < 0.03, **p < 0.0001 (ANOVA with the Bonferroni test). n ≥ 5.

All error bars, SEM.

(Chalasani et al., 2007). Laser ablation of AIB suppressed the reversal frequency to a level similar to that of AVA/AVD/AVE-ablated worms (Figure 3I). These observations raise the possibility that AIB may regulate reversal initiation by modulating RIM activity. Thus, we imaged AIB activity during reversals using the CARIBN system. AIB activity increased during reversals (Figures 3A and 3B), suggesting a role for AIB in promoting the initiation of reversals during spontaneous locomotion.

If AIB promotes reversal initiation, then stimulating AIB should trigger reversals. To test this, we expressed ChR2 as a transgene specifically in AIB. Stimulation of AIB by ChR2 effectively triggered reversals, providing further evidence for a role of AIB in promoting reversal initiation (Figure 3C).

The fact that AIB extensively synapses onto RIM suggests that AIB may act through RIM to promote the initiation of reversals. However, AIB also makes synaptic connections with other neurons, including AVA (White et al., 1986). Thus, the possibility that AIB acts through AVA rather than RIM to promote reversals cannot be ruled out. Thus, we repeated the ChR2 experiments on RIM-ablated worms and found that stimulation of AIB by ChR2 can no longer further stimulate reversals in these worms (Figure 3D). By contrast, worms with AVA/AVD/AVE ablated still initiated reversals in response to AIB stimulation by ChR2 (Figure 3E). These results suggest that under this condition, AIB acts through the RIM-dependent parallel circuit, rather than the AVA/AVD/AVE-dependent stimulatory circuit, to promote the initiation of reversals.

AIB Triggers Reversals by Inhibiting RIM

We considered that AIB may inhibit RIM to trigger reversals. This model predicts that stimulation of AIB should result in inhibition of RIM. To test this, we recorded the activity of RIM in response to AIB stimulation by ChR2. Although optogenetics has been applied to stimulate neurons in freely behaving worms (Leifer et al., 2011; Stirman et al., 2011), it has not been possible to

simultaneously record neuronal activity in the same animal. The CARIBN system allows us to stimulate one neuron by optogenetics while recording the activity of another neuron on freely behaving animals. Specifically, the blue light used to image G-CaMP calcium signals in RIM can also turn on ChR2 expressed in AIB, making it possible to image the activity of RIM in response to stimulation of AIB on freely behaving worms. Upon light stimulation, RIM exhibited a sharp decrease in calcium level (Figures 3F–3H). As predicted, worms initiated reversals (Figure 3F). The decrease in RIM activity depended on AIB stimulation because no such response was observed in worms lacking the ChR2 transgene in AIB (Figures 3G and 3H). These data, together with the results from electrophysiological recordings (see below), strongly suggest that AIB triggers reversals by inhibiting RIM activity.

Taken together, our results suggest a model in which AIB acts upstream to inhibit RIM, an inter/motor neuron that tonically inhibits reversals during locomotion; activation of AIB suppresses RIM activity, which in turn relieves the inhibitory effect of RIM on backward movement, thereby triggering reversals. In other words, backward locomotion inhibited by RIM can be ''disinhibited'' by AIB. This would constitute a disinhibitory circuit that promotes the initiation of reversals (Figure 7I).

The Disinhibitory and Stimulatory Circuits Together Form the Primary Pathways Promoting Reversal Initiation during Spontaneous Locomotion

Is this disinhibitory circuit important for the initiation of reversals during spontaneous locomotion? If so, then simultaneous elimination of both the disinhibitory and stimulatory circuits should result in a severe defect in reversal initiation. Indeed, whereas ablation of AVA/AVD/AVE or AIB only reduced reversal frequency, ablation of AVA/AVD/AVE and AIB together abolished nearly all reversal events during spontaneous locomotion (Figure 3I). These results suggest that the AIB-RIM-dependent disinhibitory circuit and the command interneurons AVA/AVD/AVE-dependent stimulatory circuit together form the primary pathways to control reversal initiation during spontaneous locomotion.

Both the Disinhibitory and Stimulatory Circuits Are Recruited to Promote the Initiation of Reversals in Response to Nose Touch

We then wondered how sensory cues impinge on these two circuits. In addition to spontaneous reversals, worms initiate reversals in response to various sensory stimuli, particularly aversive cues. As a consequence, these animals are able to avoid unfavorable or hazardous environments, a behavioral response essential for their survival. We focused on nose touch behavior, one of the best-characterized avoidance behaviors (Kaplan and Horvitz, 1993). In this behavior, touch delivered to the worm nose tip triggers reversals. The polymodal sensory neuron ASH is the primary sensory neuron detecting nose touch stimuli because its ablation leads to a severe defect in nose touch behavior (Kaplan and Horvitz, 1993). In addition, nose touch can stimulate this neuron in calcium imaging assays (Hilliard et al., 2005). Notably, ASH sends synapses to both AIB and AVA (White et al., 1986), and nose touch can excite AVA in electrophysiological assays (Mellem et al., 2002). This suggests a model in which ASH may engage both the disinhibitory and stimulatory circuits in this avoidance behavior.

To test the aforementioned model, we first employed our CARIBN system to image the activity of the nose touch circuits. Because this imaging system performs recording in an open environment, we were able to deliver touch stimuli directly to the nose tip of freely moving worms while simultaneously monitoring their neuronal activities and behavioral states. Our model predicts that nose touch should stimulate AVA but inhibit RIM via stimulating AIB. Indeed, upon nose touch, AVA showed an increase in calcium activity during reversals (Figures 4A and 4C). Similarly, nose touch also stimulated AIB during reversals (Figures 4B and 4C). By contrast, RIM was inhibited during reversals (Figures 4D and 4F). Importantly, in AIB-ablated worms, RIM was no longer inhibited during reversals, indicating that the inhibition of RIM requires AIB (Figures 4E and 4F). This is consistent with the model that sensory information flows to RIM via AIB. These observations suggest that nose touch may trigger reversals by recruiting both the disinhibitory and stimulatory circuits.

To provide additional evidence, we killed AIB, RIM, and the command interneurons. Laser ablation of AIB, RIM, or AVA/AVD/AVE all led to a significant reduction in reversal frequency (Figure 4G), indicating that both the disinhibitory and stimulatory circuits contribute to nose touch behavior. More importantly, simultaneous elimination of both circuits by killing AVA/AVD/AVE together with AIB or RIM virtually abolished all reversals triggered by nose touch (Figure 4G). Thus, the disinhibitory and stimulatory circuits together form the primary pathways through which worms initiate reversals to avoid nose touch cues.

The Disinhibitory Circuit Cooperates with the Stimulatory Circuit to Promote the Initiation of Reversals in Response to Osmotic Shock

Similar to nose touch, osmotic shock delivered to the worm nose also triggers reversals by stimulating the same sensory neuron ASH (Hilliard et al., 2005). Notably, osmotic shock is known to be much more noxious than nose touch (Mellem et al., 2002), and unlike nose touch, a failure to avoid high osmolarity environment (e.g., 4 M fructose) leads to death. As a result, osmotic shock suppressed head oscillations during reversals, whereas nose touch did not; nor was this phenomenon observed during spontaneous locomotion (Alkema et al., 2005) (Figure 5G). Suppression of head oscillations is believed to facilitate efficient escape from noxious cues such as osmotic shock, and this behavioral strategy requires stimulation of RIM (Alkema et al., 2005). As was the case with spontaneous locomotion and nose touch behavior, both AVA and AIB were stimulated by osmotic shock (Figures 5A–5C); however, RIM was stimulated rather than inhibited by osmotic shock (Figures 5D and 5F), an observation distinct from that observed in the other two behaviors. This indicates that whereas the stimulatory circuit was clearly functional in osmotic avoidance behavior, the disinhibitory circuit was instead recruited to promote suppression of head oscillations in this behavior.

To further characterize the osmotic avoidance circuits, we performed laser ablation experiments. Worms lacking the

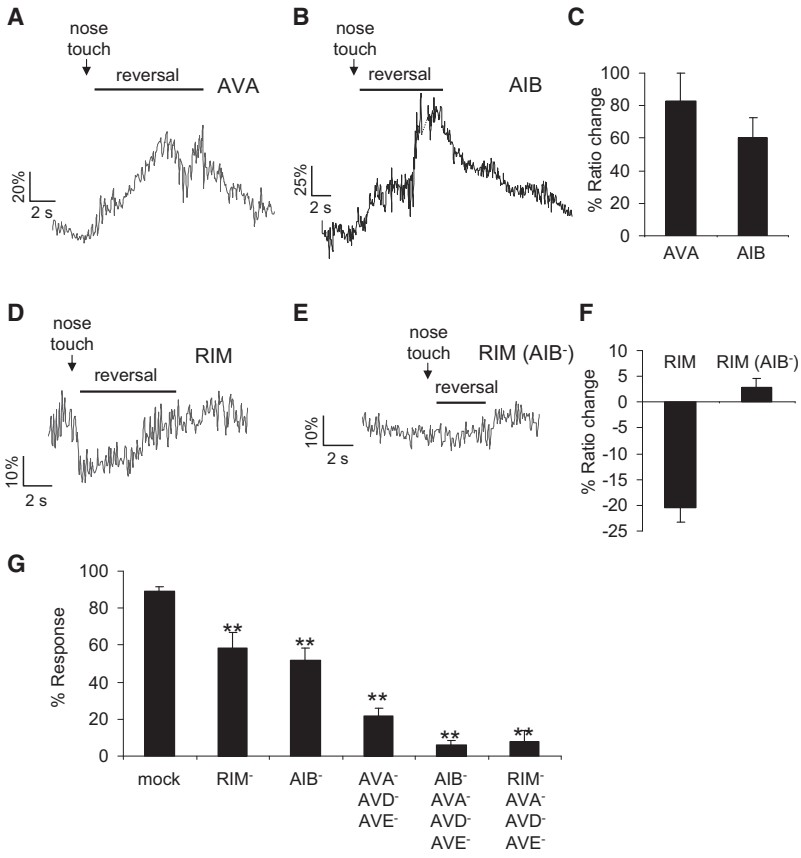

Figure 4. Worms Employ Both the Disinhibitory and Stimulatory Circuits to Trigger Backward Locomotion in Nose Touch Avoidance Behavior

(A) AVA is stimulated during reversals in nose touch behavior.

(B) AIB is stimulated during reversals in nose touch behavior. The dotted lines in the trace represent missing frames.

(C) Bar graph summarizing the data in (A) and (B) ($n \geq 11$).

(D) RIM is inhibited during reversals in nose touch behavior.

(E) Inhibition of RIM depends on AIB.

(F) Bar graph summarizing the data in (D) and (E) ($n \geq 12$).

(G) Simultaneous ablation of both the disinhibitory and stimulatory circuits abolished nearly all reversal events triggered by nose touch ($n \geq 5$). **$p < 0.0001$ (ANOVA with the Bonferroni test).

All error bars, SEM.

disinhibitory circuit (AIB or RIM ablated) only exhibited a slight, but insignificant, reduction in reversal frequency in osmotic avoidance behavior (Figure 5H). As expected, worms with RIM ablated no longer suppressed head oscillations during reversals, consistent with the role of RIM in this function (Figure 5G). By contrast, worms lacking the stimulatory circuit (AVA/AVD/AVE ablated) displayed a significant defect in osmotic avoidance behavior (Figure 5H); notably, osmotic shock can still trigger reversals in these worms, albeit at a reduced frequency, indicating that additional circuits are functional in the absence of the stimulatory circuit (Figure 5H).

We considered that the remaining reversal events in AVA/AVD/AVE-ablated worms could be mediated by the disinhibitory circuit. Indeed, in AVA/AVD/AVE-ablated worms, osmotic shock no longer stimulated RIM but, instead, inhibited RIM during reversals, which is similar to that observed in the other two behaviors (Figures 5E and 5F). This demonstrates that the disinhibitory circuit is functional in worms lacking the stimulatory circuit, suggesting that the disinhibitory circuit is responsible for the remaining avoidance response in these worms. This also suggests that the excitatory input to RIM was derived from AVA/AVD/AVE in osmotic avoidance behavior, consistent with the fact that these command interneurons form synaptic connections with RIM (White et al., 1986). Finally and importantly, simultaneous ablation of both the disinhibitory and stimulatory circuits rendered worms virtually incapable of initiating reversals in response to osmotic shock (Figure 5H). Thus, in osmotic avoidance behavior worms employ the stimulatory circuit as the primary pathway and the disinhibitory circuit as the salvage pathway to trigger reversals; in addition, worms recruit neurons in the disinhibitory circuit to suppress head oscillations to facilitate efficient escape from high osmolarity environment. This illustrates an example in which the two circuits cooperate to promote avoidance responses to noxious stimuli. This also shows that sensory cues (nose touch versus osmotic shock) differentially regulate the activity patterns of these two circuits.

Electrophysiological Recording of the Activity of the Disinhibitory and Stimulatory Circuits

Having identified the circuits that promote reversal initiation, we then set out to investigate the synaptic mechanisms by which the circuits process information. Although our CARIBN system can record the circuit activity in freely behaving animals, this assay is indirect because it measures the calcium level but not the membrane excitability of a neuron, and also lacks the capacity to resolve synaptic events in the circuitry. Thus, we decided to employ electrophysiological approaches to record the circuit activity by patch clamping. However, the small size of worm neurons (~2 μm in diameter) makes this type of recording technically challenging (Goodman et al., 1998). We focused on the nose touch circuits due to the relative ease of delivering touch stimuli with precision in whole-cell recording. This was achieved by using a glass probe driven by a piezo actuator to press the nose tip (Figure 6A).

We recorded all of the four major neurons in the two circuits: the sensory neuron ASH and the interneurons AVA, AIB, and RIM (Figure 7I). We focused on recording voltage signals through current clamp, due to the high input resistance of worm neurons (typically 2–5 GΩ) (Goodman et al., 1998; Liu et al., 2010). Nose touch evoked a depolarizing voltage

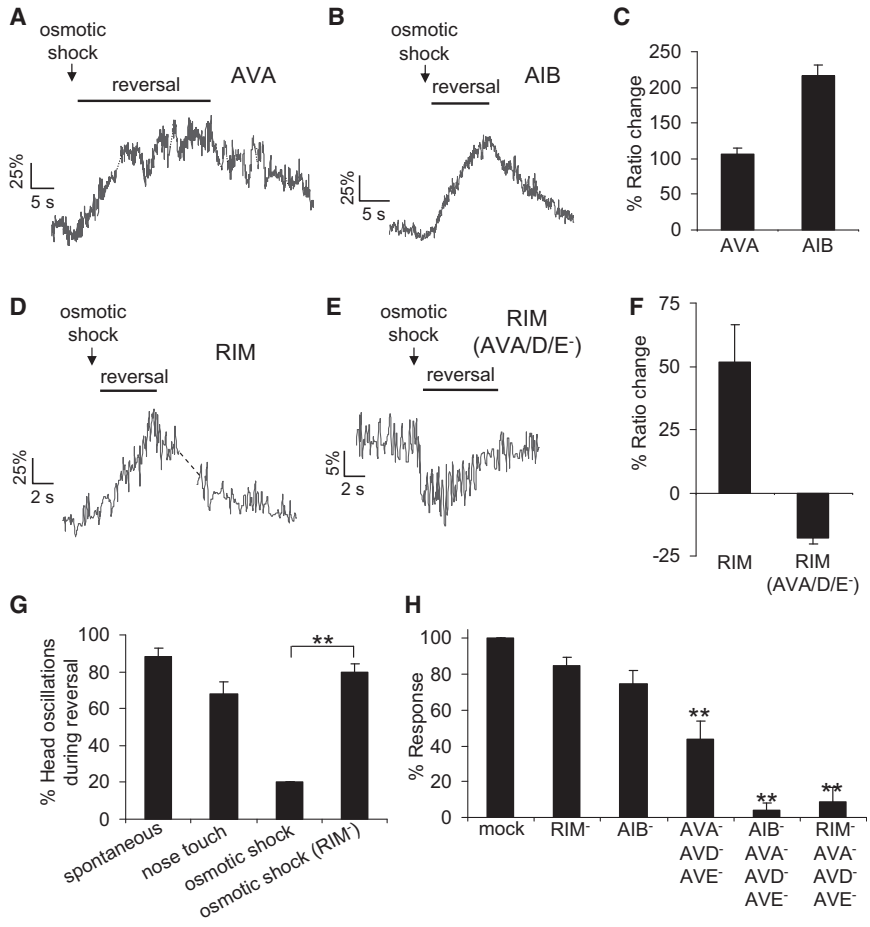

Figure 5. The Role of the Disinhibitory and Stimulatory Circuits in Triggering Backward Locomotion in Osmotic Avoidance Behavior

(A–C) AVA and AIB are stimulated during reversals in osmotic avoidance behavior. Stimulus, 2 M glycerol. $n \geq 11$.

(D) RIM is stimulated during reversals triggered by osmotic shock.

(E) RIM is inhibited during reversals in worms lacking AVA/AVD/AVE. The dotted lines in this trace and in (A) and (D) represent missing frames.

(F) Bar graph summarizing the data in (D) and (E) ($n \geq 7$).

(G) Head oscillations occur during reversals in spontaneous locomotion and nose touch behavior but are suppressed in osmotic avoidance behavior ($n = 5$). $^{**}p < 0.0001$ (ANOVA).

(H) Simultaneous ablation of both the disinhibitory and stimulatory circuits abolished nearly all reversal events triggered by osmotic shock ($n \geq 5$). $^{**}p < 0.0001$ (ANOVA with the Bonferroni test).

All error bars, SEM.

response in ASH (Figure 6B). Similarly, a depolarizing voltage signal (i.e., EPSP) was detected in AVA and AIB upon nose touch (Figures 6C–6F). By contrast, in the RIM neuron, nose touch triggered a hyperpolarizing voltage response (i.e., IPSP) (Figures 7A and 7B). Finally, we directly recorded the synaptic events between AIB and RIM by stimulating AIB with ChR2 (Figures S3A and S3B), and then recording postsynaptic responses in RIM. AIB stimulation by ChR2 led to a hyperpolarizing response (IPSP) in RIM (Figures 7C and 7D). These results are well consistent with our calcium imaging data from freely behaving animals. Thus, activation of ASH by nose touch can turn on both the disinhibitory and stimulatory circuits, providing further evidence for our model. It is worth noting that the resting potential of RIM was around −20 mV, much higher than that of AIB (∼−50 mV), indicating a more depolarized state for RIM. This is consistent with our model that RIM remains in an active state to tonically inhibit the initiation of reversals during locomotion.

The ASH-AVA and ASH-AIB Synapses Are Glutamatergic and Require an AMPA/Kainate-Type Glutamate Receptor

We first characterized the presynaptic mechanisms of the nose touch circuits. Initially, we focused on the ASH-AVA and ASH-AIB synapses. ASH is known to be glutamatergic, and worms deficient in glutamatergic transmission are severely defective in nose touch behavior (Mellem et al., 2002). Thus, we performed recordings on *eat-4* mutant worms where glutamatergic transmission is deficient. *eat-4* encodes a vesicular glutamate transporter (Lee et al., 1999). Nose touch-evoked EPSPs in AVA and AIB were severely defective in *eat-4* mutant worms (Figures 6C–6F). Furthermore, expression of wild-type *eat-4* gene in ASH restored nose touch-evoked EPSPs in AVA and AIB (Figures 6D, 6F, S2A, and S2C), as well as nose touch behavioral response in *eat-4* mutant worms (Figure 6G). These results support the view that the ASH-AVA and ASH-AIB synapses are glutamatergic.

We then turned our attention to the postsynaptic receptors, asking which glutamate receptors are required for the EPSP responses in AVA and AIB. GLR-1 is the closest *C. elegans* homolog of AMPA/kainate-type glutamate receptors and has been reported as the primary excitatory glutamate receptor in AVA and AIB (Chalasani et al., 2007; Hart et al., 1995; Maricq et al., 1995; Mellem et al., 2002). Consequently, worms lacking GLR-1 are severely defective in nose touch avoidance behavior (Hart et al., 1995; Maricq et al., 1995). We recorded the activity of AVA and AVB in response to nose touch in *glr-1* mutant worms. No EPSP signals could be evoked by nose touch in AVA or AIB of mutant worms (Figures 6C–6F), indicating that GLR-1 is required for EPSPs in these two interneurons. Furthermore, expression of wild-type *glr-1* gene in AVA or AIB restored nose touch-evoked EPSP responses in AVA or AIB of *glr-1* mutant worms, respectively (Figures 6D, 6F, S2B, and S2D), as well as nose touch behavioral responses (Figure 6G). Thus, GLR-1 is an essential subunit of the postsynaptic receptors mediating EPSPs in AVA and AIB.

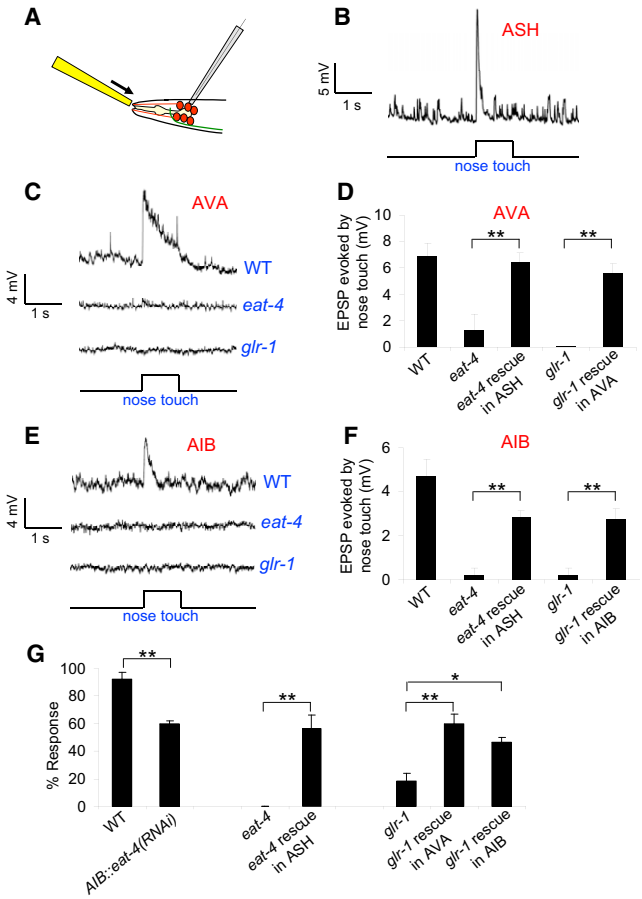

Figure 6. Electrophysiological Characterization of the ASH-AVA and ASH-AIB Synapses of the Stimulatory and Disinhibitory Circuits in Response to Nose Touch

(A) A schematic illustrating the setting of whole-cell recording (not drawn to scale).

(B) Nose touch depolarizes the sensory neuron ASH. The miniature upward spikes represent spontaneous activity of ASH. Clamping current, 0 pA.

(C and D) AVA is depolarized in response to nose touch in wild-type but not in *eat-4(ky5)* or *glr-1(n2461)* mutants ($n \geq 7$). Clamping current, 0 pA. $^{**}p < 0.005$ (t test).

(E and F) AIB is depolarized in response to nose touch, which requires *eat-4* and *glr-1* ($n \geq 5$). Clamping current, 0 pA. $^{**}p < 0.005$ (t test).

(G) Nose touch behavior ($n = 10$). $^{*}p < 0.02$; $^{**}p < 0.005$ (t tests used for two-group comparisons; ANOVA with the Dunnett test used for multi-group comparisons).

All error bars, SEM.

See also Figure S2.

The AIB-RIM Synapses Are Also Glutamatergic and Require a Glutamate-Gated Cl^- Channel

Finally, we characterized the AIB-RIM synapses. Notably, AIB also appears to be glutamatergic because it expresses *eat-4* (Ohnishi et al., 2011). As expected, nose touch can no longer trigger IPSPs in RIM of *eat-4* mutant worms (Figures 6A and 6B). However, this can also be explained by a defect in the sensory neuron ASH because *eat-4* is expressed in ASH as well. Therefore, we knocked down *eat-4* specifically in AIB by expressing an *eat-4* RNAi as a transgene specifically in AIB. RNAi of *eat-4* in AIB led to a strong deficit in nose touch-evoked IPSP in RIM (Figures 7B and S3C). This RNAi treatment also resulted in a significant defect in nose touch behavior to an extent similar to that caused by AIB ablation (Figures 6G and 4G). These data suggest that the AIB-RIM synapses are glutamatergic. To provide further evidence, we directly interrogated the AIB-RIM synapses by recording the activity of RIM in response to AIB stimulation by ChR2 in *eat-4* mutant worms. No IPSP was detected in RIM following stimulation of AIB by ChR2 in mutant worms (Figures 7C and 7D), further suggesting that the AIB-RIM synapses are glutamatergic.

The question arises as to how glutamate, a well-known excitatory neurotransmitter, triggers an inhibitory response (IPSP) in RIM. In addition to glutamate-gated cation channels such as GLR-1, the *C. elegans* genome encodes at least half a dozen glutamate-gated Cl^- channels (Yates et al., 2003). Notably, the IPSP response in RIM reversed its sign around −50 mV, close to the equilibrium potential of Cl^-, suggesting that it is mediated by a Cl^- channel (Figure S3D). Moreover, using a high Cl^- pipette solution, we detected an EPSP rather than IPSP response in RIM (Figure S3E), further suggesting that it is carried by a Cl^- channel. To provide additional evidence, we directly perfused glutamate toward RIM. Glutamate evoked a hyperpolarizing current in RIM with a reversal potential around −50 mV (Figures 7E–7G). Increasing the Cl^- concentration in the pipette solution shifted the reversal potential close to 0 mV (Figure 7G). These data together suggest that the IPSP response in RIM is mediated by a glutamate-gated Cl^- channel.

Finally, we sought to identify the glutamate-gated Cl^- channel genes required for IPSPs in RIM. We focused on the α subunits of glutamate-gated Cl^- channels because they can form functional channels on their own (Yates et al., 2003). Five such genes are present in the *C. elegans* genome, including *avr-14*, *avr-15*, *glc-1*, *glc-3*, and *glc-4* (Yates et al., 2003). Although *avr-15*, *glc-1*, *glc-3*, and *glc-4* mutant worms all expressed glutamate-gated Cl^- currents in RIM (Figure S3F), mutations in *avr-14* abolished such currents (Figures 7E and 7F). As a result, nose touch can no longer evoke IPSPs in RIM of *avr-14* mutant worms (Figure 7H). AVR-14 was expressed in RIM (Figure S3J), and expression of wild-type *avr-14* gene in RIM rescued glutamate-gated Cl^- currents (Figures 7F and S3G), as well as nose touch-evoked IPSP response in RIM (Figures S3H and S3I). Furthermore, AVR-14 can form a functional glutamate-gated Cl^- channel in heterologous systems (Dent et al., 2000). These observations indicate that AVR-14 is an essential subunit of the postsynaptic receptor(s) mediating the glutamate-gated Cl^- current underlying IPSPs in RIM.

DISCUSSION

C. elegans has emerged as a genetic model to study motor control and sensorimotor integration (de Bono and Maricq, 2005). In this study we interrogated the circuit and synaptic mechanisms underlying the initiation of reversals in spontaneous locomotion and some sensory behaviors by applying a multidisciplinary approach integrating calcium imaging, optogenetics, genetic manipulation, laser ablation, and electrophysiology.

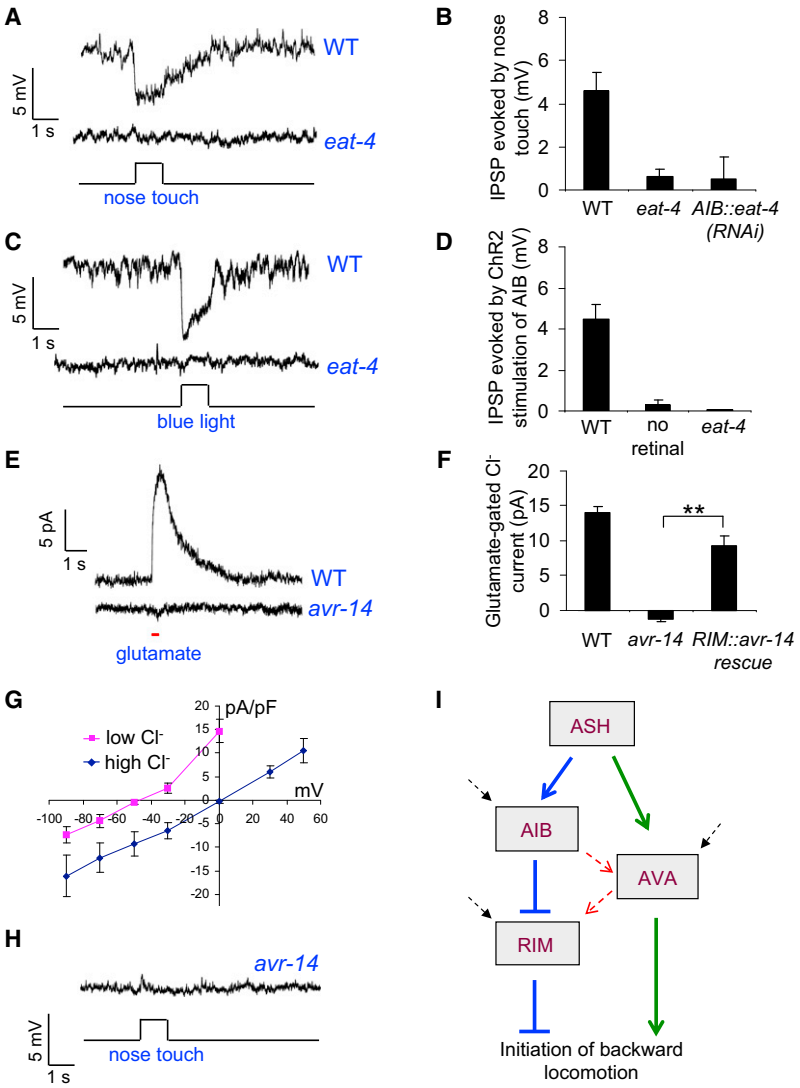

Figure 7. Electrophysiological Characterization of the AIB-RIM Synapse of the Disinhibitory Circuit in Response to Nose Touch

(A and B) RIM is hyperpolarized in response to nose touch, which depends on *eat-4*. n ≥ 9. Clamping current, 0 pA.

(C and D) AIB stimulation by ChR2 leads to inhibition of RIM. See AIB traces in Figure S3A. n ≥ 6. Clamping current, 0 pA.

(E and F) Glutamate (1 mM) perfusion evokes a hyperpolarizing outward current in RIM, which was absent in *avr-14(ad1302)* mutant worms. Voltage clamp, 0 mV. The small inward current in *avr-14(ad1302)* mutant was carried by an unknown glutamate-gated cation channel whose activity was masked by the predominant anion channel AVR-14 in wild-type worms (n ≥ 6). **p < 0.001 (t test).

(G) Glutamate-gated currents are carried by a Cl^- channel (n = 5).

(H) No IPSP signal was detected in RIM of *avr-14(ad1302)* mutant worms in response to nose touch. Clamping current, 0 pA.

(I) A schematic model illustrating the disinhibitory and stimulatory circuits. The dotted arrows in red indicate crosstalk between the two circuits. AIB, if overstimulated by ChR2 (with >10× brighter blue light), also sends output to AVA (B.J.P., J.L., and X.Z.S.X., unpublished data). The dotted arrows in black indicate that other unknown sensory neurons and interneurons may regulate the two circuits by sending output to AVA, AIB, and RIM.

All error bars, SEM.

See also Figure S3.

Performing calcium imaging and optogenetic assays on freely behaving worms allowed us to reliably associate circuit activity with behavior. Genetic manipulation and laser ablation facilitated the interrogation of the role of individual genes and neurons in the circuitry. The use of electrophysiology enabled us to validate the circuitry and also to dissect the synaptic mechanisms by which the circuitry processes information. A combination of these approaches permits a rigorous dissection of the neural and genetic basis of behavior. To our knowledge, such a comprehensive approach has not been applied to map neural circuits underlying behavior in other organisms.

We found that our current model of *C. elegans* locomotion circuitry needs to be significantly revised. In particular we showed that the command interneurons AVA/D/E, which were long believed to be essential for the initiation of reversals, are in fact not required for this motor program. Genetic ablation of these neurons and others also suggested a similar conclusion (Zheng et al., 1999). Importantly, we identified an RIM inter/motor neuron-dependent disinhibitory circuit acting in concert with the command interneuron-mediated stimulatory circuit to promote the initiation of reversals (Figure 7I). RIM may control reversal initiation by regulating the activity of its downstream motor neurons and/or muscles, and possibly the command interneurons that control forward movement (e.g., AVB and PVC). The presence of two circuits may help ensure that this critical motor program be efficiently executed, and also provide flexibility for its modulation by sensory inputs and perhaps by experience.

These two circuits apparently do not act in isolation and are regulated by sensory cues. In addition to ASH, other sensory neurons may impinge on these circuits. Other interneurons may also modulate these circuits via AVA/D/E, RIM, and AIB (Figure 7I). For example AIZ and AIY form connections with RIM and may regulate RIM activity. Finally, the two circuits may regulate each other through crosstalk as shown in osmotic avoidance behavior. It should also be noted that our data do not exclude the possibility that additional circuits may function in parallel to regulate reversals. One interesting observation is that though connected by gap junctions, the activity patterns of RIM and AVA are not synchronized in spontaneous locomotion or nose touch behavior, suggesting that these electrical synapses are dynamically regulated under different physiological contexts. Similar observations have been observed in vertebrate retinal circuits (Bloomfield and Völgyi, 2009). This presents an example in which distinct sensory inputs (nose

touch versus osmotic shock) differentially regulate the dynamics of motor circuits. Future studies will elucidate whether and how other sensory cues, sensory neurons, and interneurons regulate these two circuits, how they regulate each other through cross-talk, and whether and how they are modulated by experience.

Interestingly, the disinhibitory circuit identified in this study is functionally analogous to those found in the mammalian basal ganglia that facilitate the initiation of motor programs. These circuits allow the brain to suppress competing or nonsynergistic motor programs that would otherwise interfere with sensory and goal-directed behaviors (Purves et al., 2008). In the case of *C. elegans*, because its pharynx cannot efficiently take up surrounding bacteria (i.e., worm food) during backward locomotion, such a circuit would provide a potential mechanism for the animal to suppress reversals; in doing so the animal would be able to spend most of its time moving forward or dwelling to facilitate feeding and only initiate reversals stochastically (spontaneous reversals) or in response to sensory cues.

Stimulatory circuits have also been widely employed by mammals to control motor initiation (Purves et al., 2008). For example, in response to painful sensory stimuli, nociceptive DRG neurons can bypass the basal ganglia and the upper motor nervous system to trigger a limb withdrawal response by directly activating the local circuitry in the spinal cord (Purves et al., 2008). This would ensure that animals can rapidly escape from painful stimuli (Purves et al., 2008). In the case of *C. elegans*, the disinhibitory circuit functions in spontaneous locomotion and nose touch behavior. Interestingly, when encountering more noxious stimuli (e.g., osmotic shock), worms also bypass the disinhibitory circuit and primarily depend on the stimulatory circuit to trigger reversals. Our results suggest that despite the great diversity of their anatomy, the nervous systems from distantly related organisms may adopt similar strategies to control motor output.

Conclusions

As the only organism with a structural map of the entire nervous system available, *C. elegans* has emerged as a model to dissect how genes and neural circuits generate behavior (de Bono and Maricq, 2005). Nevertheless, much of the information regarding motor circuits was inferred from the structural map and, thus, has not been extensively tested at the experimental level. It has become increasingly clear that a structural map of the nervous system, though highly informative, cannot be directly transcribed into a functional map (de Bono and Maricq, 2005). Apparently, an understanding of the functional map requires rigorous interrogation of the functional roles of individual neurons in the circuitry in the context of behavior and of how genes, environment and experience regulate circuit dynamics and hence behavioral output. Our study illustrates an example of how a multidisciplinary approach can be employed to study these questions in a genetic model organism.

EXPERIMENTAL PROCEDURES

The CARIBN System and Calcium Imaging

As diagramed in Figure 1B, the automated CARIBN system consists of an upright microscope (Zeiss M2Bio), EMCCD camera (Andor), dual-view beamsplitter (Optical Insights), Xenon light source (Sutter), motorized stage, and computer (Dell). A C-mount (0.63×) is used to couple the camera to the beamsplitter. A dual-band excitation filter (Chroma) simultaneously excites G-CaMP and DsRed at 488 and 560 nm, respectively. This system can be readily adapted to monitor fluorescent signals from Cameleon that has also been extensively used for imaging calcium transients in *C. elegans* neurons and muscles (Clark et al., 2006; Faumont and Lockery, 2006; Kerr et al., 2000). In this case a different set of filters is needed. We used a 20× objective in conjunction with a 1.6× zoom lens to acquire images. A home-developed software package controls the system and follows fluorescent objects (neurons of the worm) in dark field by their size and brightness. Specifically, a feedback loop system is introduced to track the object (neurons of the worm) by instructing the stage to move the object to the center of the camera field (recentering) every half second (2 Hz). Under this setting we very rarely (<1%) lose track of the worm over a 10 min window. Images were acquired with 10–30 ms exposure time (depending on fluorescence intensity of the transgene) at up to 22 Hz without binning. To facilitate identification of neurons for ratio computation, a mask image was generated for each frame by applying the following digital filters: a spatial filter to sharpen the image by correcting the motion blur; and an intensity filter and size filter to single out the neuron of interest from other neurons and the nerve ring. None of these digital filters would alter the ratio of G-CaMP/DsRed fluorescence because the ratio computation was solely based on the raw images. Nevertheless, there are always a few frames, particularly those captured during stage movement, that are of poor image quality; thus, these frames are not processed and are marked with dotted lines in the traces. A series of digital spatial filters and morphological filters were used to selectively enhance the autofluorescence emitted from the worm body, such that the outline of the worm body (head and a portion of the anterior body) can be identified to derive behavioral parameters such as backward/forward movement, speed, and trajectory. To compute the ratio change during a reversal event, we first determined the precise starting and ending frame numbers of the reversal. The image data ~2 s before the starting frame were used as the basal line, and the mean ratio value of this basal line was used to compute the ratio change. The first peak or trough within the reversal period was identified to calculate the ratio change.

Calcium imaging was performed on day 1 adult worms under the standard laboratory condition where worms were allowed to freely move on the surface of an NGM plate covered with a thin layer of bacteria (OP50) without any physical restraint. Nose touch stimulus was delivered as described (Kaplan and Horvitz, 1993). A small drop of 2 M glycerol was placed on the path of a forward-moving worm to induce osmotic avoidance response as described (Mellem et al., 2002). OP50 was not included in the osmotic assay. A positive response was scored if the worm stopped forward movement and also initiated a reversal lasting at least half of a head swing. We only scored the reversals initiated within the first 3 s after the animal encountered the drop. Each worm was tested five times with an ~5 min interval between each test, and a percent score was tabulated for each worm. To image the activity of RIM in response to ChR2 stimulation by ChR2, worms were first tracked under the DsRed channel excited with yellow light and then switched to the G-CaMP/DsRed channels excited with both blue and yellow light. To control intrinsic phototaxis responses (Ward et al., 2008), imaging was performed on *lite-1(xu7)* worms insensitive to blue light (Liu et al., 2010).

Optogenetics

Worms grown on NGM plates supplied with 5 μM all-trans retinal were tested on retinal-free NGM plates spread with a thin layer of OP50. ChR2 experiments were carried out in *lite-1(xu7)* worms lacking intrinsic phototaxis responses (Liu et al., 2010). Unless otherwise indicated, a 5 s pulse of blue (470 ± 20 nm; 0.1–0.2 mW/mm^2) or yellow light (575 ± 25 nm; 25 mW/mm^2) was delivered from an Arc lamp (EXFO) by a 10× objective (Zeiss M2Bio) to the head of a forward-moving worm to turn on ChR2 or NpHR, respectively. A positive response was scored if the worm stopped forward movement and also initiated a reversal at least than half of a head swing. We only scored the reversals initiated during the 5 s of light illumination. Each worm was tested five times with an ~5 min interval between each test, and a percent score was tabulated for each worm. Because worms exhibit spontaneous reversals, a basal level of reversals was observed in controls. This number shows some variation, which

may be contributed by temperature, humidity, and quality of NGM plates. Because worms reared on retinal-containing plates show a slightly higher frequency of spontaneous reversals under our conditions, transgene-free siblings (rather than worms grown on retinal-free plates) were used as controls in behavioral tests.

Electrophysiology

Patch-clamp recordings were performed under an Olympus microscope (BX51WI) using an EPC-10 amplifier and the Pulse software (HEKA) as previously described (Kang et al., 2010). Briefly, we glued worms to a Sylgard-coated coverglass covered with bath solution and then carefully cut a small piece of cuticle in the head to expose head neurons while keeping the nose tip intact. The animal was kept alive during recording. To preserve synaptic functions, it is important to avoid displacing neurons from their original position during dissection; otherwise, chemical synapses may get disrupted/depressed, and their activity may also quickly run down (though electric synapses tend to be preserved). Blue light pulses (0.2 mW/mm^2; 470 ± 20 nm; 0.5–1 s) were delivered from an Arc lamp (EXFO Xcite) coupled to a mechanical shutter (Sutter) triggered by the amplifier. A glass probe driven by a piezo actuator (PI) mounted on a micromanipulator was used to deliver nose touch stimuli (10 μm) toward the nose tip. The normal bath solution contains: 145 mM NaCl, 5 mM KCl, 1 mM $CaCl_2$, 5 mM $MgCl_2$, 11 mM dextrose, and 5 mM HEPES (330 mOsm; pH adjusted to 7.3). The pipette solution contains 115 mM K-gluconate, 15 mM KCl, 5 mM $MgCl_2$, 10 mM HEPES, 0.25 mM $CaCl_2$, 20 mM sucrose, 5 mM EGTA, 5 mM Na_2ATP, and 0.5 mM NaGTP. When recording nose touch- and ChR2-evoked responses, supernatant from freshly grown OP50 culture was diluted (1:10) into the bath solution to mimic the conditions of behavioral assays and also to help prevent the run down of synaptic functions. In the high Cl^- pipette solution, 115 mM K-gluconate was replaced with KCl. Cells were mostly recorded by current clamp, and currents were clamped at 0 pA unless otherwise indicated.

Molecular Genetics and Laser Ablation

Standard methods were used to generate plasmids and transgenes driven by cell-specific promoters. Laser ablation was also conducted using standard protocols. See Extended Experimental Procedures for details.

SUPPLEMENTAL INFORMATION

Supplemental Information includes Extended Experimental Procedures, three figures, and one movie and can be found with this article online at doi:10.1016/j.cell.2011.08.053.

ACKNOWLEDGMENTS

We thank J. Gao, W. Li, W. Zhou, and A. Ward for technical assistance; L. Looger for the G-CaMP3.0 plasmid; A. Gottschalk for ChR2 plasmid; K. Deisseroth for NpHR plasmid; J. Dent and L. Avery for *avr-14* strains and plasmids; and P. Hu, A. Kumar, and B. Ye for comments on the manuscript. Some strains were obtained from the CGC and Knockout Consortiums in the USA and Japan. B.J.P. was supported by a predoctoral T32 training grant from the NEI (University of Michigan). This work was supported by grants from the NIGMS and Pew scholar program (to X.Z.S.X.).

Received: March 25, 2011
Revised: June 18, 2011
Accepted: August 25, 2011
Published: November 10, 2011

REFERENCES

Alkema, M.J., Hunter-Ensor, M., Ringstad, N., and Horvitz, H.R. (2005). Tyramine Functions independently of octopamine in the *Caenorhabditis elegans* nervous system. Neuron *46*, 247–260.

Ben Arous, J., Tanizawa, Y., Rabinowitch, I., Chatenay, D., and Schafer, W.R. (2010). Automated imaging of neuronal activity in freely behaving *Caenorhabditis elegans*. J. Neurosci. Methods *187*, 229–234.

Bloomfield, S.A., and Völgyi, B. (2009). The diverse functional roles and regulation of neuronal gap junctions in the retina. Nat. Rev. Neurosci. *10*, 495–506.

Boyden, E.S., Zhang, F., Bamberg, E., Nagel, G., and Deisseroth, K. (2005). Millisecond-timescale, genetically targeted optical control of neural activity. Nat. Neurosci. *8*, 1263–1268.

Chalasani, S.H., Chronis, N., Tsunozaki, M., Gray, J.M., Ramot, D., Goodman, M.B., and Bargmann, C.I. (2007). Dissecting a circuit for olfactory behaviour in *Caenorhabditis elegans*. Nature *450*, 63–70.

Chalfie, M., Sulston, J.E., White, J.G., Southgate, E., Thomson, J.N., and Brenner, S. (1985). The neural circuit for touch sensitivity in *Caenorhabditis elegans*. J. Neurosci. *5*, 956–964.

Clark, D.A., Biron, D., Sengupta, P., and Samuel, A.D. (2006). The AFD sensory neurons encode multiple functions underlying thermotactic behavior in *Caenorhabditis elegans*. J. Neurosci. *26*, 7444–7451.

de Bono, M., and Bargmann, C.I. (1998). Natural variation in a neuropeptide Y receptor homolog modifies social behavior and food response in *C. elegans*. Cell *94*, 679–689.

de Bono, M., and Maricq, A.V. (2005). Neuronal substrates of complex behaviors in *C. elegans*. Annu. Rev. Neurosci. *28*, 451–501.

Dent, J.A., Smith, M.M., Vassilatis, D.K., and Avery, L. (2000). The genetics of ivermectin resistance in *Caenorhabditis elegans*. Proc. Natl. Acad. Sci. USA *97*, 2674–2679.

Faumont, S., and Lockery, S.R. (2006). The awake behaving worm: simultaneous imaging of neuronal activity and behavior in intact animals at millimeter scale. J. Neurophysiol. *95*, 1976–1981.

Feng, Z., Li, W., Ward, A., Piggott, B.J., Larkspur, E.R., Sternberg, P.W., and Xu, X.Z.S. (2006). A *C. elegans* model of nicotine-dependent behavior: regulation by TRP-family channels. Cell *127*, 621–633.

Goodman, M.B., Hall, D.H., Avery, L., and Lockery, S.R. (1998). Active currents regulate sensitivity and dynamic range in *C. elegans* neurons. Neuron *20*, 763–772.

Gray, J.M., Hill, J.J., and Bargmann, C.I. (2005). A circuit for navigation in *Caenorhabditis elegans*. Proc. Natl. Acad. Sci. USA *102*, 3184–3191.

Guo, Z.V., Hart, A.C., and Ramanathan, S. (2009). Optical interrogation of neural circuits in *Caenorhabditis elegans*. Nat. Methods *6*, 891–896.

Hart, A.C., Sims, S., and Kaplan, J.M. (1995). Synaptic code for sensory modalities revealed by *C. elegans* GLR-1 glutamate receptor. Nature *378*, 82–85.

Hilliard, M.A., Apicella, A.J., Kerr, R., Suzuki, H., Bazzicalupo, P., and Schafer, W.R. (2005). In vivo imaging of *C. elegans* ASH neurons: cellular response and adaptation to chemical repellents. EMBO J. *24*, 63–72.

Kang, L., Gao, J., Schafer, W.R., Xie, Z., and Xu, X.Z.S. (2010). *C. elegans* TRP family protein TRP-4 is a pore-forming subunit of a native mechanotransduction channel. Neuron *67*, 381–391.

Kaplan, J.M., and Horvitz, H.R. (1993). A dual mechanosensory and chemosensory neuron in *Caenorhabditis elegans*. Proc. Natl. Acad. Sci. USA *90*, 2227–2231.

Kerr, R., Lev-Ram, V., Baird, G., Vincent, P., Tsien, R.Y., and Schafer, W.R. (2000). Optical imaging of calcium transients in neurons and pharyngeal muscle of *C. elegans*. Neuron *26*, 583–594.

Lee, R.Y., Sawin, E.R., Chalfie, M., Horvitz, H.R., and Avery, L. (1999). EAT-4, a homolog of a mammalian sodium-dependent inorganic phosphate cotransporter, is necessary for glutamatergic neurotransmission in *caenorhabditis elegans*. J. Neurosci. *19*, 159–167.

Leifer, A.M., Fang-Yen, C., Gershow, M., Alkema, M.J., and Samuel, A.D. (2011). Optogenetic manipulation of neural activity in freely moving *Caenorhabditis elegans*. Nat. Methods *8*, 147–152.

Liu, J., Ward, A., Gao, J., Dong, Y., Nishio, N., Inada, H., Kang, L., Yu, Y., Ma, D., Xu, T., et al. (2010). *C. elegans* phototransduction requires a G protein-dependent cGMP pathway and a taste receptor homolog. Nat. Neurosci. *13*, 715–722.

Liu, K.S., and Sternberg, P.W. (1995). Sensory regulation of male mating behavior in *Caenorhabditis elegans*. Neuron *14*, 79–89.

Maricq, A.V., Peckol, E., Driscoll, M., and Bargmann, C.I. (1995). Mechanosensory signalling in *C. elegans* mediated by the GLR-1 glutamate receptor. Nature *378*, 78–81.

Mellem, J.E., Brockie, P.J., Zheng, Y., Madsen, D.M., and Maricq, A.V. (2002). Decoding of polymodal sensory stimuli by postsynaptic glutamate receptors in *C. elegans*. Neuron *36*, 933–944.

Mori, I., and Ohshima, Y. (1995). Neural regulation of thermotaxis in *Caenorhabditis elegans*. Nature *376*, 344–348.

Nagel, G., Brauner, M., Liewald, J.F., Adeishvili, N., Bamberg, E., and Gottschalk, A. (2005). Light activation of channelrhodopsin-2 in excitable cells of *Caenorhabditis elegans* triggers rapid behavioral responses. Curr. Biol. *15*, 2279–2284.

Ohnishi, N., Kuhara, A., Nakamura, F., Okochi, Y., and Mori, I. (2011). Bidirectional regulation of thermotaxis by glutamate transmissions in *Caenorhabditis elegans*. EMBO J. *30*, 1376–1388.

Purves, D., Augustine, G.J., Fitzpatrick, D., Hall, W.C., LaMantia, A.-S., McNamara, J.O., and White, L.E. (2008). Movement and its central control. In Neuroscience, Fourth Edition (Sunderland, MA: Sinauer Associates, Inc.), pp. 397–541.

Raizen, D.M., Zimmerman, J.E., Maycock, M.H., Ta, U.D., You, Y.J., Sundaram, M.V., and Pack, A.I. (2008). Lethargus is a *Caenorhabditis elegans* sleep-like state. Nature *451*, 569–572.

Reigl, M., Alon, U., and Chklovskii, D.B. (2004). Search for computational modules in the *C. elegans* brain. BMC Biol. *2*, 25.

Sporns, O., and Kötter, R. (2004). Motifs in brain networks. PLoS Biol. *2*, e369.

Stirman, J.N., Crane, M.M., Husson, S.J., Wabnig, S., Schultheis, C., Gottschalk, A., and Lu, H. (2011). Real-time multimodal optical control of neurons and muscles in freely behaving *Caenorhabditis elegans*. Nat. Methods *8*, 153–158.

Tian, L., Hires, S.A., Mao, T., Huber, D., Chiappe, M.E., Chalasani, S.H., Petreanu, L., Akerboom, J., McKinney, S.A., Schreiter, E.R., et al. (2009). Imaging neural activity in worms, flies and mice with improved GCaMP calcium indicators. Nat. Methods *6*, 875–881.

Ward, A., Liu, J., Feng, Z., and Xu, X.Z. (2008). Light-sensitive neurons and channels mediate phototaxis in *C. elegans*. Nat. Neurosci. *11*, 916–922.

White, J.G., Southgate, E., Thomson, J.N., and Brenner, S. (1986). The structure of the nervous system of the nematode *Caenorhabditis elegans*. Philos. Trans. R. Soc. Lond. B Biol. Sci. *314*, 1–340.

Yates, D.M., Portillo, V., and Wolstenholme, A.J. (2003). The avermectin receptors of Haemonchus contortus and *Caenorhabditis elegans*. Int. J. Parasitol. *33*, 1183–1193.

Zhang, F., Wang, L.P., Brauner, M., Liewald, J.F., Kay, K., Watzke, N., Wood, P.G., Bamberg, E., Nagel, G., Gottschalk, A., and Deisseroth, K. (2007). Multimodal fast optical interrogation of neural circuitry. Nature *446*, 633–639.

Zheng, Y., Brockie, P.J., Mellem, J.E., Madsen, D.M., and Maricq, A.V. (1999). Neuronal control of locomotion in *C. elegans* is modified by a dominant mutation in the GLR-1 ionotropic glutamate receptor. Neuron *24*, 347–361.

Cell

EXTENDED EXPERIMENTAL PROCEDURES

Laser Ablation

Laser ablations were performed on L1 or L2 worms (Bargmann and Avery, 1995). The transgene *Pnmr-1::gfp* was included in worms to help identify AVA, AVD, AVE and RIM (Brockie et al., 2001). To quantify reversals, we assayed day 1 adult worms (10 min) on NGM plates spread with a thin layer of OP50 bacteria using an automated worm tracking system described previously (Feng et al., 2006). A positive score was assigned if both the head and the tail of a worm moved backwards for at least half of a head swing. Most ablations shown in the same panel were done in parallel. To make data collected from different days comparable, the same mock controls were repeated every time. Only those ablations with similar control data were considered comparable.

Molecular Genetics

Plasmids encoding G-CaMP and DsRed2 (Clontech) driven by the *nmr-1* promoter were co-injected to generate transgenic lines co-expressing G-CaMP and DsRed, which were used for imaging of AVA (Brockie et al., 2001). The transgenes *AIB::ChR2::YFP, AIB::G-CaMP/DsRed, AIB::glr-1, AIB::eat-4(RNAi)* were driven by the *npr-9* promoter (Bendena et al., 2008), and the transgene *RIM::NpHR::YFP* and *RIM::avr-14* were controlled by the *gcy-13* promoter (Ortiz et al., 2006). To capture all the *avr-14* iso-forms, the *avr-14* rescuing construct was made as a mini-gene by fusing a cDNA fragment encoding the first six common exons with a genomic fragment encompassing the rest of the gene. The transgene expressing *eat-4* RNAi was generated by injecting two separate (sense and anti-sense) constructs encompassing a fragment of *eat-4* gene in N2 as described previously (Harris et al., 2010). The *cex-1* promoter was used to drive expression in RIM of the transgene *RIM::G-CaMP/DsRed* (Colon-Ramos et al., 2007). We confirmed by cell position that the *cex-1* promoter is expressed in RIM. The transgene *ASH::eat-4* was expressed under the *sra-6* promoter (Troemel et al., 1995). The two transgenic arrays *AIB::ChR2::YFP* and *RIM::G-CaMP/DsRed* were crossed together for calcium imaging of RIM in response to AIB stimulation using the CARIBN system. For patch-clamp recordings, ASH, AVA, AIB and RIM was each marked with a transgene expressing mCherry (or DsRed) under the *sra-6, nmr-1, npr-9* and *gcy-13* promoter, respectively. These transgenes were crossed together with others (e.g. rescuing, ChR2 and RNAi transgenes) to mark neurons for recording. G-CaMP3.0 was used in all cases for calcium imaging except in RIM (G-CaMP1.3).

SUPPLEMENTAL REFERENCES

Bargmann, C.I., and Avery, L. (1995). Laser killing of cells in Caenorhabditis elegans. Methods Cell Biol. *48*, 225–250.

Bendena, W.G., Boudreau, J.R., Papanicolaou, T., Maltby, M., Tobe, S.S., and Chin-Sang, I.D. (2008). A Caenorhabditis elegans allatostatin/galanin-like receptor NPR-9 inhibits local search behavior in response to feeding cues. Proc. Natl. Acad. Sci. USA *105*, 1339–1342.

Brockie, P.J., Madsen, D.M., Zheng, Y., Mellem, J., and Maricq, A.V. (2001). Differential expression of glutamate receptor subunits in the nervous system of Caenorhabditis elegans and their regulation by the homeodomain protein UNC-42. J. Neurosci. *21*, 1510–1522.

Colon-Ramos, D.A., Margeta, M.A., and Shen, K. (2007). Glia promote local synaptogenesis through UNC-6 (netrin) signaling in C. elegans. Science *318*, 103–106.

Feng, Z., Li, W., Ward, A., Piggott, B.J., Larkspur, E., Sternberg, P.W., and Xu, X.Z.S. (2006). A C. elegans model of nicotine-dependent behavior: regulation by TRP family channels. Cell *127*, 621–633.

Harris, G., Mills, H., Wragg, R., Hapiak, V., Castelletto, M., Korchnak, A., and Komuniecki, R.W. (2010). The monoaminergic modulation of sensory-mediated aversive responses in Caenorhabditis elegans requires glutamatergic/peptidergic cotransmission. J. Neurosci. *30*, 7889–7899.

Ortiz, C.O., Etchberger, J.F., Posy, S.L., Frokjaer-Jensen, C., Lockery, S., Honig, B., and Hobert, O. (2006). Searching for neuronal left/right asymmetry: genome-wide analysis of nematode receptor-type guanylyl cyclases. Genetics *173*, 131–149.

Troemel, E.R., Chou, J.H., Dwyer, N.D., Colbert, H.A., and Bargmann, C.I. (1995). Divergent seven transmembrane receptors are candidate chemosensory receptors in C. elegans. Cell *83*, 207–218.

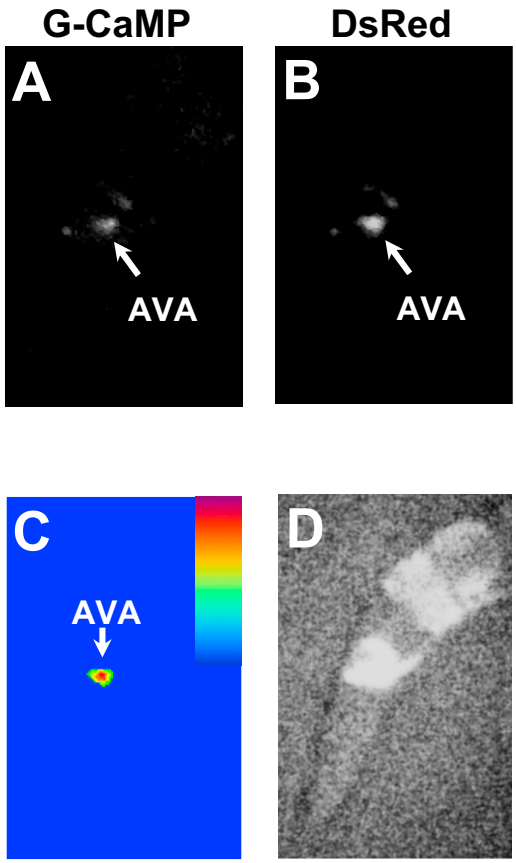

Figure S1. Sample Images Acquired by the CARIBN System, Related to Figures 2, 3, 4, and 5

(A) A snapshot raw image of a freely-moving worm under the G-CaMP channel. The arrow points to the AVA neuron. The worm harbors a transgene co-expressing G-CaMP and DsRed2 under the *nmr-1* promoter. Images were acquired with 5 ms exposure time at 22 Hz without binning.

(B) Raw image of the same animal from the same frame under the DsRed channel.

(C) G-CaMP/DsRed ratio image processed from (A) and (B). Digital filters were applied to mask other neurons and the nerve ring in the image to facilitate ratio computation. Pseudocolor was generated to indicate the relative ratio.

(D) An enhanced image of (B) allowing for visualization of the worm body. Digital filters were applied to selectively enhance the autofluorescence of the worm body.

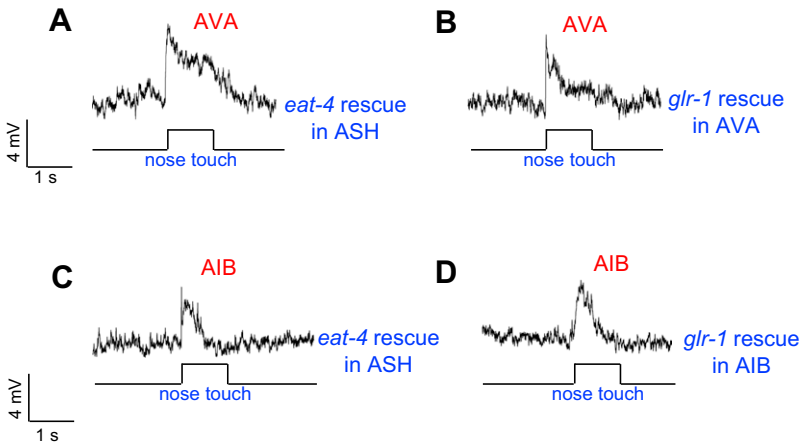

Figure S2. Sample Traces of AVA and AIB EPSP Responses Evoked by Nose Touch, Related to Figure 6

(A and B) AVA traces. Expression of wild-type *eat-4* gene in the presynaptic neuron ASH under the *sra-6* promoter rescues nose touch-evoked EPSP response in AVA of *eat-4* mutant worms (A). Expression of wild-type *glr-1* gene in AVA rescues nose touch-evoked EPSP response in AVA of *glr-1* mutant worms (B). See data summary in Figure 6D.

(C and D) AIB traces. Expression of wild-type *eat-4* gene in the presynaptic neuron ASH under the *sra-6* promoter rescues nose-touch evoked EPSP response in AIB of *eat-4* mutant worms (C). Expression of wild-type *glr-1* gene in AIB under the *npr-9* promoter rescues nose touch-evoked EPSP response in AIB of *glr-1* mutant worms (D). See data summary in Figure 6F.

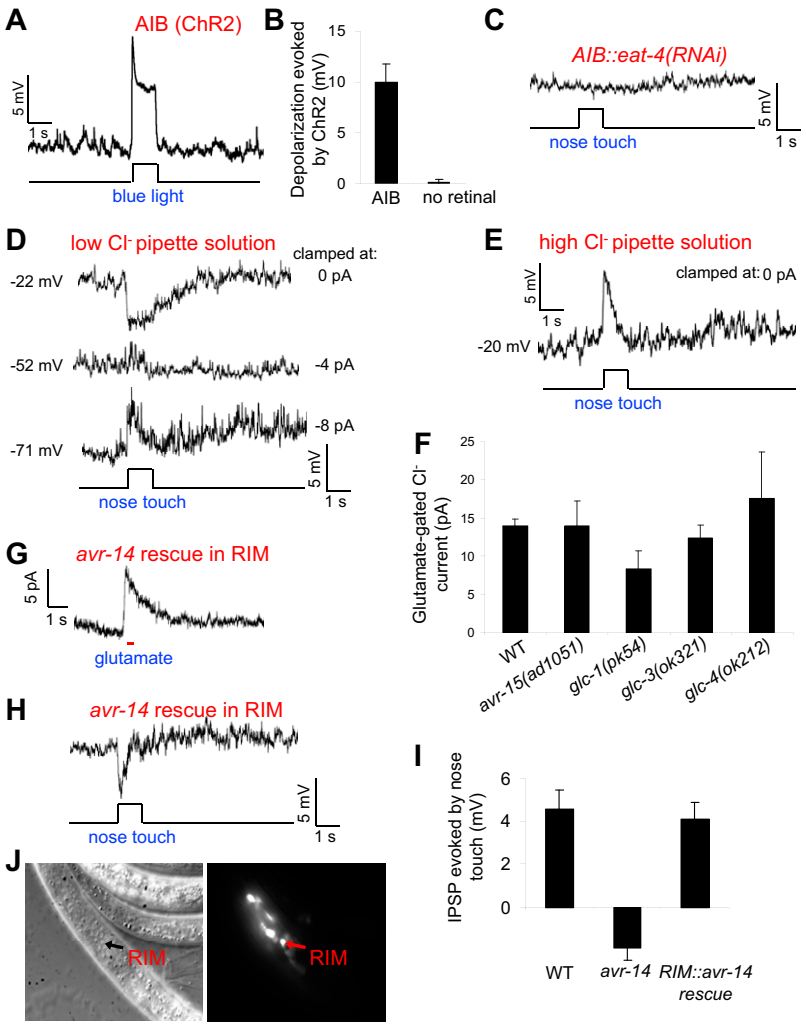

Figure S3. Additional Characterizations of the AIB-RIM Synapses of the Disinhibitory Circuit in Response to Nose Touch, Related to Figure 7

(A and B) ChR2 stimulation by blue light depolarizes AIB. ChR2 was expressed as a transgene specifically in AIB under the *npr-9* promoter. Error bars: SEM. n ≥ 7. No depolarization response was observed in control worms (no retinal). n≥5. Error bars: SEM. Clamping current: 0 pA.

(C) RNAi of *eat-4* in AIB abolishes the RIM IPSP signal evoked by nose touch. Sample trace. Clamping current: 0 pA. RNAi was expressed as a transgene in AIB under the *npr-9* promoter. See data summary in Figure 7B.

(D and E) The IPSP response in RIM is mediated by a Cl- channel. (D) The IPSP response in RIM reversed its sign around -50 mV under low Cl- pipette solution. Clamping currents were indicated to the right of the traces, and the resulting voltages were marked to the left. (E) Nose touch evoked an EPSP rather than IPSP under high Cl- pipette solution.

(F) Glutamate-gated Cl- currents in RIM of mutant worms lacking genes encoding the alpha-subunits of glutamate-gated Cl- channels. Recordings were performed as described in Figure 7E. Clamping voltage: 0 mV. Error bars: SEM.

(G and H) Sample traces of rescued RIM responses in *avr-14* mutant. (G) Glutamate-gated Cl- current in RIM of *avr-14* mutant worms was rescued by expression of wild-type *avr-14* gene in RIM under the *gcy-13* promoter. Clamping voltage: 0 mV. See data summary in Figure 7F. (H) The same transgene rescues the RIM IPSP response evoked by nose touch. Clamping current: 0 pA.

(I) Bar graph summarizing the data in (H) and Figure 7H. Similar to that described in Figure 7F, *avr-14* mutant worms showed a small depolarizing response which was carried by an unknown glutamate-gated cation channel whose activity was masked by the predominant anion channel AVR-14 in wild-type. n≥8. The WT data from Figure 7B is also included. Error bars: SEM.

(J) *avr-14* is expressed in RIM. A 7 kb PCR product encompassing 2.9 kb 5UTR and 4.2 kb coding region of the *avr-14* gene was amplified from genomic DNA and fused to YFP driven by a SL2 trans-splicing site. Left: DIC image; right: fluorescence image. Arrows point to RIM.